Buckling Analysis of Axially Loaded Corrugated Cylindrical Shells

Xin Ning * and Sergio Pellegrino†

California Institute of Technology, Pasadena, CA 91125

Buckling analyses of heavily corrugated cylindrical shells based on detailed full finite element models are usually computationally expensive. To address this issue, we have proposed an efficient computational method of predicting the onset of buckling for corrugated cylindrical shells which builds on the Bloch wave method for infinitely periodic structures. We modified the traditional Bloch wave method in order to analyze the buckling of rotationally periodic shell structures. We have developed an efficient algorithm to perform our modified Bloch wave method. The buckling behavior of composite corrugated cylindrical shells with a range of numbers of corrugations was analyzed. Linear and nonlinear buckling analyses of detailed full finite element models were also performed and compared to our method. Comparisons showed that our modified Bloch wave method was able to obtain highly accurate buckling loads and it was able to capture both global and local buckling modes. It was also found that the computational time required by our modified Bloch wave method did not scale up as the number of corrugations increased.

I. Introduction

Corrugated shells have been widely used over decades as aerospace, civil and naval structures such as rocket and aircraft shells, ship panels, roof panels, cores of sandwich structures, etc. Corrugated shells are stiff in the longitudinal direction along corrugations, enabling them to carry longitudinal loads with high mass efficiency [1]. Compared to their longitudinal stiffness, corrugated shells are relatively compliant transverse to the corrugation direction. This anisotropic property has been recently exploited and led to their applications as flexible or morphing wings [2, 3].

Although current commercial finite element codes allow us to analyze the buckling behavior of corrugated shells, simulations on detailed finite element models could be very computational expensive. In practice, the dimensions of corrugated shells are much larger than the period and amplitude of corrugations. For example, the corrugated shell designed by Johnson [1] has a diameter of 3 meters, whereas the period and amplitude of its corrugations are only 11.4 and 1.1 centimeters, respectively. Therefore, it is necessary to use very small elements to mesh the corrugations in order to obtain accurate results, leading to heavy finite element analyses. The high computational effort has been the major constraint on the use of finite element analysis in the optimization of corrugated/stiffened shells [4].

A variety of methods have been introduced to reduce the computational costs of buckling analysis of corrugated shells. A common approach is to replace the exact corrugated cross-section with a smooth shell that has equivalent stiffness properties. The smeared-out method is a simple method to compute the equivalent properties, and it has been used in the buckling analysis of both stiffened and corrugated shells since 1960s [1, 5–7]. In the smeared-out method the discrete stiffeners or corrugations are distributed over the original shell surface by adding an equivalent continuous layer, and then calculations are preformed on the uniform but anisotropic shell [8].

Motivated by recent studies on morphing wings, various homogenization methods have been developed to obtain more rigorous equivalent stiffness properties than the smeared-out method for corrugated shells,

*Graduate Student. Graduate Aerospace Laboratories, California Institute of Technology, 1200 E. California Blvd. MC 105-50. xning@caltech.edu

†Joyce and Kent Kresa Professor of Aeronautics and Professor of Civil Engineering, Graduate Aerospace Laboratories, California Institute of Technology, 1200 E. California Blvd. MC 301-46. AIAA Fellow. sergiop@caltech.edu

see Refs. [9–12]. In the homogenization methods strains and curvatures are applied independently on a single corrugation and, utilizing the periodicity of corrugated shells, the corresponding reaction forces and moments on the corrugation boundaries are analytically or numerically computed. The equivalent stiffness properties are then calculated through the load-displacement relations.

Both the smeared-out and homogenization methods can reduce the computational costs of finite element models because fine meshes are no longer required due to the simple geometry of the equivalent shells. However, these two methods are valid only when the buckling is global, i.e. the wave length of the buckling mode is much larger than the period of corrugations or stiffeners [4,8]. They cannot be used to capture local skin or stiffener buckling or to calculate stresses [13].

In 1980s Williams and co-workers developed a stiffness matrix method for the buckling and vibration analysis of corrugated and stiffened shells which treats the shells as assemblages of flat plates that are connected along their common longitudinal edges [14–17]. The stiffness matrices in this method are computed based on the flat plate theory, and the buckling loads and modes are obtained by solving the corresponding eigenproblems. The program VIPASA was developed based on the stiffness matrix method, and it was found that VIPASA is much more efficient than general-purpose finite element programs [17, 18]. VIPASA can analyze both flat and cylindrical corrugated and stiffened shells.

A unique feature of the stiffness matrix method by Williams and co-workers is that, based on the periodicity of corrugated or stiffened shells, the buckling mode of a repetitive portion can be expressed as a product of a complex-valued exponential term times the buckling mode of any other repetitive portion [19, 20]. This relation makes it possible to condense the full stiffness matrix of the whole shell into a smaller matrix of only a single repetitive portion. However, this method can only analyze corrugated/stiffened shells made of flat plates. Shells with curved walls, e.g. sinusoidally corrugated shells, must be approximated by a series of flat panels. In addition, it should be noted that the buckling modes are assumed to vary sinusoidally along the corrugations in this method. Therefore, this method could provide inaccurate results if the shells are short and clamped in the longitudinal direction.

In 1990s Triantafyllidis and co-workers developed the Bloch wave method for the buckling analysis of infinitely periodic structures [21–23]. It has been one of the major tools for the buckling analysis of cellular structures such as honeycombs [24], porous solids [25], and foams [26]. This method is based on the assumption that the buckling modes of a infinitely periodic structure follow the form of the Bloch wave propagation which is the product of a complex-valued plane wave exponential term times a function with the periodicity of one repetitive unit cell [27]. The buckling loads and modes can be computed by performing eigenvalue analyses on a single unit cell whose boundaries are coupled by the Bloch relations rather on the whole structure, resulting in the reduction of computational costs.

We propose an efficient computational method for the buckling analysis of corrugated cylindrical shells in this paper that builds on the stiffness matrix method and the Bloch wave method. We modified the Bloch wave method based on the work by Williams and co-workers to make it applicable for the buckling analysis of rotationally periodic structures. We also implemented the modified Bloch wave method in Abaqus and developed an efficient algorithm to perform the computation.

The paper is organized as follows. Section II reviews the stiffness matrix method for rotationally periodic structures and the theory of Bloch wave method. The modified Bloch wave method for corrugated cylindrical shells is presented in Section III. The method of implementing the Bloch wave method in Abaqus and the algorithm of finding the critical buckling loads are presented in Section IV. We applied our modified Bloch wave method to analyze the buckling behavior of corrugated composite cylindrical shells with various numbers of corrugations. The results are presented and compared to the linear and nonlinear full finite element analyses in Section V. Section VI concludes the paper.

II. Background

A brief review on the stiffness matrix method for the buckling analysis of rotationally periodic structures is first presented, followed by the theory of Bloch wave method. The similarities and differences between these two methods are also discussed. The reader is referred to Refs. [14–17] and Refs. [21–23] for extensive details of the stiffness matrix method and Bloch wave method, respectively.

A. Stiffness Matrix Method for Rotationally Periodic Structures

A buckling problem can be expressed as an eigenvalue problem:

$$K_c(\lambda)\tilde{U}_c = 0 \tag{1}$$

where K_c is the complete global stiffness matrix of a structure, and $\tilde{U}_c$ is its eigenvector which is also the buckling mode. λ is the critical buckling load factor which is the load or displacement applied on the structure. For a rotationally periodic structure, such as the ones shown in Fig. 1, with N repetitive portions, $\tilde{U}_c$ can be separated into

$$\tilde{U}_c = [\tilde{U}_1, \tilde{U}_2, \tilde{U}_3, ..., \tilde{U}_N]^T \tag{2}$$

where $\tilde{U}_q$ is the eigenvector of the q^{th} portion of the structure. Due to the rotational periodicity, the stiffness matrix has the following form [19]:

$$K_c(\lambda) = \begin{bmatrix} K_1 & K_2 & K_3 & \dots & K_N \\ K_N & K_1 & K_2 & \dots & K_{N-1} \\ K_{N-1} & K_N & K_1 & \dots & K_{N-2} \\ \vdots & \vdots & \vdots & \vdots & \vdots \\ K_2 & K_3 & K_4 & \dots & K_1 \end{bmatrix} \tag{3}$$

where K_q is the stiffness matrix corresponding to the q^{th} portion of the structure. Let the degree of freedom of a repetitive portion be J, then K_q is a $J \times J$ matrix.

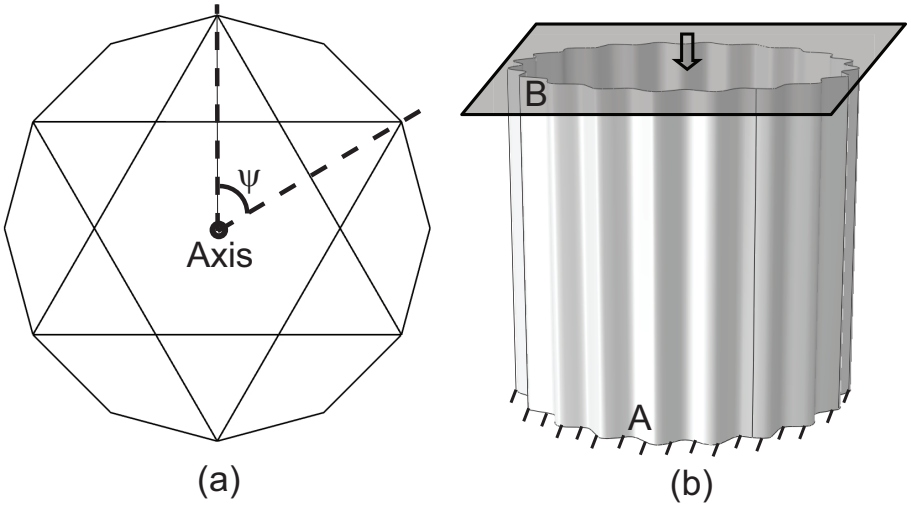

Figure 1: (a) A rotationally periodic 2D truss structure with 6 repetitive portions. ψ is the angle spanned by a repetitive portion which is $\pi/3$ in this example. (b) A rotationally periodic cylindrical truss structure. The nodes on edge "A" or "B" are "axis nodes", i.e. they have the same deformation. [20]

Hence, Eq. 1 can be written as a set of m equations:

$$\Sigma_{q=1}^{N} K_q(\lambda)\tilde{U}_{m+q-1} = 0, \quad m = 1, 2, 3, ...N \tag{4}$$

where the eigenvectors must satisfy the following relation due to the rotational periodicity:

$$\tilde{U}_{q+N} = \tilde{U}_q \tag{5}$$

The most general solution to Eqs. 4 and 5 is [19]

$$\tilde{U}_q = \tilde{U}_1 e^{i(q-1)n\psi} \tag{6}$$

with $i = \sqrt{-1}$, $n = 0, 1, 2, ..., N$, and $\psi = 2\pi/N$. Substitute Eq. 6 into Eq. 4 and divide it by $e^{imn\psi}$, we can reduce the set of m equations into the same equation:

$$(\Sigma_{q=1}^{N} K_q(\lambda)e^{i(q-1)n\psi})\tilde{U}_1 = 0, \qquad n = 0, 1, 2, 3, ...N \tag{7}$$

It should be noted that

$$e^{i(q-1)(N-n)\psi} = e^{-i(q-1)n\psi} \tag{8}$$

Therefore, n and $N-n$ are not independent and the range of n can be reduced to $n = 1, 2, 3, ...\{N/2\}$, where $\{N/2\}$ is the largest integer no larger than $N/2$.

The eigenvalue problem in Eq. 1 of the complete stiffness matrix K_c of the whole structures are separated into $\{N/2\}+1$ eigenvalue problems of $\Sigma_{q=1}^{N} K_q(\lambda)e^{i(q-1)n\psi}$ which has the same dimension as the stiffness matrix of only one repetitive portion of the structure. The displacement vector $\tilde{U}_i$ is complex-valued. Hence, both the real and imaginary parts of $\tilde{U}_i$ are possible buckling modes. However, when $n = 0$ or $n = N/2$ for even N, the exponential term in Eq. 6 is a real value. There is only one buckling mode corresponding to these two cases. The critical buckling load is the lowest one among the buckling loads for all n's.

$$\lambda_{crit} = \min_{n=0,1,...,\{N/2\}} (\lambda(n)) \tag{9}$$

It is very common for rotationally periodic structures to have "axis nodes", i.e. nodes sheared by all the repeating portions or have the same translational and rotational deformation with respect to the axis, as shown in Fig. 1 (b). For example, stiffened or corrugated cylindrical shells subject to axial uniform end-shortening have "axis nodes" on their two ends. Let $\tilde{U}_{Zq}$ be the displacement w.r.t axis Z of the "axis nodes" of the q^{th} portion, and substitute it into Eq. 6:

$$\tilde{U}_{Zq} = \tilde{U}_{Z1}e^{i(q-1)n\psi}, \qquad n = 0, 1, 2, 3, ...\{N/2\} \tag{10}$$

Because the nodes are "axis nodes", $\tilde{U}_{Zq}$ must satisfy $\tilde{U}_{Zq} = \tilde{U}_{Z1}$. Therefore, $\tilde{U}_{Zq}$ is always zero for $n > 0$.

B. Bloch Wave Method

The Bloch wave method [21–26] is a robust and efficient way of predicting the onset of buckling for infinitely periodic structures. In this section we briefly review the theory of the Bloch wave method for a two-dimensional infinitely periodic structures. A unit cell of this structure is shown in Fig. 2. Let $K(\lambda)$ be the stiffness matrix of the unit cell, and then the equilibrium equation of buckling can be written as:

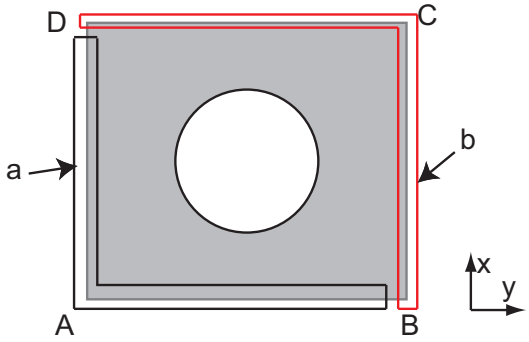

Figure 2: Schematic of a unit cell of a 2D infinitely periodic porous structure. A, B, C, and D are four points on the corners of the unit cell. Region "a" includes edges "AD", "AB", and point A; region "b" includes edges "CD", "BC", and points B, C, and D.

$$K(\lambda)\tilde{U} = \tilde{F} \tag{11}$$

where $\tilde{U}$ and $\tilde{F}$ are the buckling modes and the corresponding force vector. It should be noted that $\tilde{F}$ is not zero. However, if Eq. 11 of each unit cell is assembled into the complete stiffness of the whole structure, the complete force vector of the whole structure is zero when buckling happens, as seen in Eq. 1.

$\tilde{U}$ and $\tilde{F}$ can be separated into the values on boundary and internal nodes:

$$\begin{aligned} \tilde{U} &= [\tilde{U}_i, \tilde{U}_a, \tilde{U}_b]^T \\ \tilde{F} &= [\tilde{F}_i, \tilde{F}_a, \tilde{F}_b]^T \end{aligned} \tag{12}$$

where i, a and b denote the internal nodes, nodes in regions "a" and "b", respectively, as shown in Fig. 11. Therefore, the displacements and forces of regions "a" and "b" are:

$$\begin{aligned}\tilde{U}_a &= [\tilde{U}_{(AD)}, \tilde{U}_A, \tilde{U}_{(AB)}]^T \\ \tilde{F}_a &= [\tilde{F}_{(AD)}, \tilde{F}_A, \tilde{F}_{(AB)}]^T \\ \tilde{U}_b &= [\tilde{U}_B, \tilde{U}_{(BC)}, \tilde{U}_C, \tilde{U}_{(CD)}]^T \\ \tilde{F}_b &= [\tilde{F}_B, \tilde{F}_{(BC)}, \tilde{F}_C, \tilde{F}_{(CD)}]^T\end{aligned} \tag{13}$$

The notation $(*)$ means edges without their end nodes.

Because of the periodicity of the structure, the buckling mode and the corresponding force can be assumed to follow the Bloch wave propagation function:

$$\begin{aligned}\tilde{U}(x,y) &= P_u(x,y)exp[i(\frac{n_1}{L_1}x + \frac{n_2}{L_2}y)] \\ \tilde{F}(x,y) &= P_f(x,y)exp[i(\frac{n_1}{L_1}x + \frac{n_2}{L_2}y)]\end{aligned} \tag{14}$$

where L_j and n_j/L_j, $j = 1, 2$ are the sizes of the unit cell and the wave numbers. $P_u(x,y)$ and $P_f(x,y)$ are periodic functions with the same periodicity as a unit cell:

$$\begin{aligned}P_u(x,y) &= P_u(x + m_1L_1, y + m_2L_2) \\ P_f(x,y) &= P_f(x + m_1L_1, y + m_2L_2)\end{aligned} \tag{15}$$

where m_1 and m_2 are integers. Using Eqs. 14 and 15, we can obtain the following Bloch relations for the displacements on the boundary nodes:

$$U_B = \mu_1 U_A; \;\; U_{(BC)} = \mu_1 U_{(AD)}; \;\; U_C = \mu_1 U_D; \;\; U_C = \mu_2 U_B; \;\; U_{(CD)} = \mu_2 U_{(AB)}; \;\; U_D = -\mu_2 U_A \tag{16}$$

where $\mu_1 = exp(in_1)$ and $\mu_2 = exp(in_2)$. Similarly, the forces on the boundaries have the following Bloch relations:

$$F_B = -\mu_1 F_A; \;\; F_{(BC)} = -\mu_1 F_{(AD)}; \;\; F_C = -\mu_1 F_D; \;\; F_C = -\mu_2 F_B; \;\; F_{(CD)} = -\mu_2 F_{(AB)}; \;\; F_D = -\mu_2 F_A \tag{17}$$

Using Eq. 16, the displacements can be written as:

$$[\tilde{U}_i, \tilde{U}_{(AD)}, \tilde{U}_A, \tilde{U}_{(AB)}, \tilde{U}_B, \tilde{U}_{(BC)}, \tilde{U}_C, \tilde{U}_{(CD)}]^T = Q[\tilde{U}_i, \tilde{U}_{(AD)}, \tilde{U}_A, \tilde{U}_{(AB)}]^T \tag{18}$$

where the transformation matrix Q is:

$$\begin{bmatrix} \mathbf{I} & \mathbf{0} & \mathbf{0} & \mathbf{0} \\ \mathbf{0} & \mathbf{I} & \mathbf{0} & \mathbf{0} \\ \mathbf{0} & \mathbf{0} & \mathbf{I} & \mathbf{0} \\ \mathbf{0} & \mathbf{0} & \mathbf{0} & \mathbf{I} \\ \mathbf{0} & \mathbf{0} & [\mu_1] & \mathbf{0} \\ \mathbf{0} & [\mu_1] & \mathbf{0} & \mathbf{0} \\ \mathbf{0} & \mathbf{0} & [\mu_1\mu_2] & \mathbf{0} \\ \mathbf{0} & \mathbf{0} & \mathbf{0} & [\mu_2] \end{bmatrix} \tag{19}$$

The notation $[*]$ represents a submatrix of Q. Substitute Eq. 19 into Eq. 11, multiply it by Q^T, and use Eq. 17, we can obtain:

$$Q^T K(\lambda) Q \tilde{U}_a = \hat{K}(n_1, n_2, \lambda)\tilde{U}_a = Q^T \tilde{F} = 0 \tag{20}$$

Therefore, the buckling load and mode can be obtained by solving the eigenvalue problem of matrix $\hat{K}$. It should be noted that $\hat{K}$ also depends on the n_1 and n_2; hence, the buckling load factor λ is a function of n_1 and n_2:

$$\lambda = \lambda(n_1, n_2) \tag{21}$$

The critical buckling load is obtained by finding the lowest λ for all possible n_1 and n_2.

$$\lambda_{crit} = \min_{n_1,n_2}(\lambda(n_1, n_2)) \tag{22}$$

The Bloch wave relations in Eqs. 16 and 17 are complex-valued functions. However, most finite element packages, including Abaqus, cannot handle complex-valued fields. Therefore, the stiffness matrices K and $\hat{K}$ in most Bloch wave analyses are analytically formulated, and the calculations are very difficult and tedious. To address this issue, Gong et. al. [26] used Abaqus to extract the element stiffness matrices and then assembled them into the stiffness matrix of a unit cell. It was pointed out by the authors that this procedure could be very time-consuming if the geometry of the unit cell is intricate. Aberg and Gudmundson [28] invented an alternative technique for studying the wave dispersion relations of infinitely periodic structures that used two identical meshes in Abaqus to split the complex-valued fields into real and imaginary parts. The boundaries of the two meshes were coupled in order to satisfy the Bloch wave relations. Following Aberg and Gudmundson [28], Bertoldi et. al. [25, 29] introduced this technique in the buckling analysis of porous periodic elastomeric structures. More details of applying the Bloch wave method in Abaqus are presented in Section IV.

Recently, the Bloch wave method was introduced in the buckling analysis of stiffened cylindrical shells by Wang and Abdalla [30]. They used the Bloch wave method to find the local buckling loads and modes of stiffened shells, whereas the global buckling was predicted through a homogenized stiffness model. The Bloch wave method for infinite periodic structures was used, i.e. the local buckling analysis was performed on a unit repetitive grid that is assumed to be in a circumferentially and axially infinite stiffened cylindrical shell. Therefore, the boundary conditions were essentially not considered in Wang and Abdalla [30].

C. Comparison between the Stiffness Matrix Method and the Bloch Wave Method

The stiffness matrix method for rotationally periodic structures and the Bloch wave method for infinitely periodic structures have similar features. First, both methods achieve the reduction of computational costs by separating the eigenproblem of the whole structure into a series of smaller eigenproblems which involve stiffness matrix with the same dimension as the matrix of a single unit cell. Second, the assumed buckling mode relations among repeating portions in the stiffness matrix method (Eq. 6) are essentially the same as the Bloch wave relations in Eq. 16.

However, these two methods formulate the eigenproblems in different ways. The stiffness matrix method involves the stiffness matrices of all the repetitive portions of a rotationally periodic structure, as shown in Eq. 7. The stiffness matrix in the Bloch wave method involves only a single unit cell, and the boundaries of the unit cell are coupled by the Bloch wave relations to transform the equilibrium equation (11) of a unit cell into an eigenproblem, as seen in Eq. 20.

III. Methodology

We tailored the Bloch wave method based on the stiffness matrix method for rotationally periodic structures in order to apply the Bloch wave method in the buckling analysis of corrugated cylindrical shells. The methodology is presented in this section.

A. Bloch Wave Method for Corrugated Cylindrical Shells subject to Axial Compression

Corrugated cylindrical shells are periodic only in the circumferential direction, as shown in Fig. 3. The shell is compressed by applying a uniform end-shortening on one of its ends. Hence, Eq. 14 can be reduce into the following relation for corrugated shells:

$$\begin{aligned} \tilde{U}(z,\phi) &= P_u(z,\phi)exp(ik\phi) \\ \tilde{F}(z,\phi) &= P_f(z,\phi)exp(ik\phi) \end{aligned} \tag{23}$$

z and ϕ denote the shell axial coordinate and angular position in the circumferential direction. k is the wave number. Let the angle spanned by a corrugation be ψ, we have:

$$\tilde{U}(z,\phi+\psi) = P_u(z,\phi+\psi)e^{ik(\phi+\psi)} = P_u(z,\phi)e^{ik\phi}e^{ik\psi} = \tilde{U}(z,\phi)e^{ik\psi} \tag{24}$$

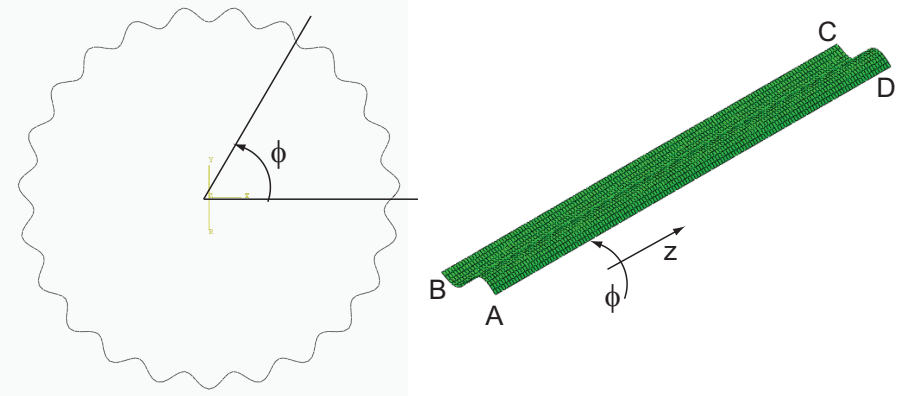

Figure 3: (a) Cross-section of a corrugated cylindrical shell. (b) Perspective view of a corrugation. ϕ and z are the circumferential and axial directions, respectively. A, B, C, and D are four points on the corners of the corrugation

When $\phi = 0$, Eq. 24 is written as:

$$\tilde{U}(z,\psi) = \tilde{U}(z,0)e^{ik\psi} \tag{25}$$

Eq. 25 means that the displacement field on the right edge of the corrugation is always the product of the displacement field on the left edge times an exponential term $e^{ik\psi}$. It should be noted that Williams also obtained this relation in Ref. [19], although it was not refereed to as the Bloch relation.

For a rotationally periodic structures with N repetitive portions, the following constraint must be satisfied: [19]

$$\tilde{U}(z,N\psi) = \tilde{U}(z,0) \tag{26}$$

Using the Bloch wave relation (Eq. 25), the above equation is now:

$$\tilde{U}(z,N\psi) = \tilde{U}(z,0) = \tilde{U}(z,0)e^{ikN\psi} \tag{27}$$

We can have:

$$e^{ikN\psi} = 1 \tag{28}$$

Therefore,

$$k\psi = \frac{2\pi}{N}n, \quad n = 0,1,2,...,N \tag{29}$$

Using Eq. 29, the Bloch relation Eq. 25 can be written as:

$$\tilde{U}(z,\psi) = \tilde{U}(z,0)\ exp(i\frac{2\pi}{N}n), \quad n = 0,1,2,...,N \tag{30}$$

Similarly, the Bloch relation for force vectors is

$$\tilde{F}(z,\psi) = -\tilde{F}(z,0)\ exp(i\frac{2\pi}{N}n), \quad n = 0,1,2,...,N \tag{31}$$

By the symmetry of the above relation:

$$\tilde{U}(z,0)\ exp(i\frac{2\pi}{N}(N-n)) = \tilde{U}(z,0)\ exp(-i\frac{2\pi}{N}n) \tag{32}$$

The wave numbers $N-n$ and n are a pair of same waves propagating in the opposite directions and they have the same buckling loads and modes. Therefore, only the following n's are necessary in the buckling analysis:

$$n = 0,1,2,...,\{N/2\} \tag{33}$$

where $\{N/2\}$ is $N/2$ for even N and $(N-1)/2$ for odd N.

Let the circumferential coordinate of edges "AD" and "BC" be 0 and ψ, respectively. $\tilde{U}$ and $\tilde{F}$ are the eigenvector and corresponding force vector of a corrugation:

$$\begin{aligned}\tilde{U} &= [U_i, U_{(AB)}, U_{(CD)}, U_{[AD]}, U_{[BC]}]^T \\ \tilde{F} &= [F_i, F_{(AB)}, F_{(CD)}, F_{[AD]}, F_{[BC]}]^T\end{aligned} \tag{34}$$

The notations $(*)$ and $[*]$ represent edges without and with nodes on their nodes. The Bloch relations Eqs. 30 and 31 are now:

$$\begin{aligned}\tilde{U}_{[BC]} &= \tilde{U}_{[AD]}\ exp(i\frac{2\pi}{N}n), \quad n = 0, 1, 2, ..., \{N/2\} \\ \tilde{F}_{[BC]} &= -\tilde{F}_{[AD]}\ exp(i\frac{2\pi}{N}n), \quad n = 0, 1, 2, ..., \{N/2\}\end{aligned} \tag{35}$$

The equilibrium equation of a corrugation during buckling is

$$K(\lambda)[U_i, U_{(AB)}, U_{(CD)}, U_{[AD]}, U_{[BC]}]^T = [F_i, F_{(AB)}, F_{(CD)}, F_{[AD]}, F_{[BC]}]^T \tag{36}$$

The stiffness matrix $K(\lambda)$ and force vector $[F_i, F_{(AB)}, F_{(CD)}, F_{[AD]}, F_{[BC]}]^T$ in Eq. 36 can be assembled into the global stiffness and force vector of the whole corrugated shell, and the following eigenproblem can be obtained:

$$K_c(\lambda)\tilde{U}_c = \tilde{F}_c = 0 \tag{37}$$

where K_c and U_c are the global stiffness matrix and the eigenvector of the whole structure. $\tilde{F}_c$ is zero when the structure buckles. Note that the force vectors F_i, $F_{(AB)}$, and $F_{(CD)}$ remain unchanged when they are assembled into the force vector in Eq. 37 because the edges "(AB)", "(CD)", and internal nodes do not interact with the nodes in other corrugations. Therefore, Eq. 36 can be written as:

$$K(\lambda)[U_i, U_{(AB)}, U_{(CD)}, U_{[AD]}, U_{[BC]}]^T = [0, 0, 0, F_{[AD]}, F_{[BC]}]^T \tag{38}$$

Similar to Eq. 18, the incremental displacements on edge "AD" can be eliminated by the following relation:

$$[U_i, U_{(AB)}, U_{(CD)}, U_{[AD]}, U_{[BC]}]^T = Q[U_i, U_{(AB)}, U_{(CD)}, U_{[AD]}]^T \tag{39}$$

where Q is

$$Q = \begin{bmatrix} \mathbf{I} & \mathbf{0} & \mathbf{0} & \mathbf{0} \\ \mathbf{0} & \mathbf{I} & \mathbf{0} & \mathbf{0} \\ \mathbf{0} & \mathbf{0} & \mathbf{I} & \mathbf{0} \\ \mathbf{0} & \mathbf{0} & \mathbf{0} & \mathbf{I} \\ \mathbf{0} & \mathbf{0} & \mathbf{0} & [exp(i\frac{2\pi}{N}n)] \end{bmatrix} \tag{40}$$

Let $[U_i, U_{(AB)}, U_{(CD)}, U_{[AD]}]^T = \tilde{U}_a$, and similar to Eq. 20, we can obtain the following eigenproblem:

$$Q^T K(\lambda) Q \tilde{U}_a = \hat{K}(n, \lambda)\tilde{U}_a = Q^T \tilde{F} = 0, \quad n = 0, 1, 2, ..., \{N/2\} \tag{41}$$

where λ is the loading factor. The critical buckling load are the lowest one among all buckling loads for n's

$$\lambda_{crit} = \min_{n=0,1,2,...,\{N/2\}}(\lambda(n)) \tag{42}$$

B. Buckling and Natural Frequency Analysis

Operationally, the eigenvalue analysis of the buckling problem in Eq. 41 is solved by analyzing the corresponding natural frequency problem. This is based on the fact that buckling happens when the lowest natural frequency decreases to zeros as the loading increases [31]. The equation of motion of a corrugation for a natural frequency problem is:

$$M\ddot{\tilde{u}} + K\tilde{u} = \tilde{F} \tag{43}$$

where M and K are mass and stiffness matrices, respectively. $\tilde{u}$ is the complex-valued displacement field and $\ddot{\tilde{u}}$ denotes its second derivative with respect to time t. The displacement can be written as:

$$\tilde{u} = \tilde{U}e^{i\omega t} \tag{44}$$

where ω is the angular frequency. Substitute Eq. 44 into 43, multiply it by Q^T, use the relation in Eq. 39, and eliminate the exponential term, we obtain the following relation:

$$Q^T(K - \omega^2 M)Q\tilde{U}_a = 0 \tag{45}$$

Therefore, Eq. 45 is an eigenvalue problem, and the eigenvalue ω^2 and eigenvector $\tilde{U}$ are respectively square of nature frequency and vibration mode. If the lowest natural frequency is zero, i.e. $\omega^2 = 0$, Eq. 45 degenerates into the eigenproblem in Eq. 41. The buckling problem can be solved through the natural frequency problem by finding the load when the lowest natural frequency is zero. The vibration mode of the frequency problem in this case is also the buckling mode.

When the eigenvalue ω^2 is positive, the angular frequency ω is a real value. $\tilde{u}$ can be written as

$$\tilde{u} = \tilde{U}e^{i\omega t} = \tilde{U}(cos(\omega t) + isin(\omega t)) \tag{46}$$

However, when $\omega^2 < 0$, ω is a complex value and $e^{i\omega t}$ exponentially grows with time, leading to an unstable structure. Therefore, $\omega^2 = 0$ corresponds to the onset of buckling and this relation is exploited to facilitate the implementation of the Bloch wave method in Abaqus.

IV. Numerical Implementation

Most of current commercial finite element packages, including Abaqus, cannot deal with complex-valued fields. We modified the technique developed by Aberg and Gudmundson [28] and Bertoldi et. al. [25, 29] to apply our modified Bloch wave method in Abaqus. Our technique is first presented in this section, followed by an efficient algorithm of finding the critical buckling loads and modes.

A. Finite Element Implementation

The complex-valued fields can be separated into real and imaginary parts, and the equation of motion of a corrugation (Eq. 43) can be written as

$$\left(\begin{bmatrix} K & \mathbf{0} \\ \mathbf{0} & K \end{bmatrix} - \omega^2 \begin{bmatrix} M & \mathbf{0} \\ \mathbf{0} & M \end{bmatrix} \right) \begin{bmatrix} \tilde{U}^{Re} \\ \tilde{U}^{Im} \end{bmatrix} = \begin{bmatrix} \tilde{F}^{Re} \\ \tilde{F}^{Im} \end{bmatrix} \tag{47}$$

where $\tilde{U}^{Re}$, $\tilde{U}^{Im}$, $\tilde{F}^{Re}$, and $\tilde{F}^{Im}$ are the real and imaginary parts of the displacement and force fields of a corrugation. The complex Bloch relation of displacements in Eq. 35 can be separated into two equations, each of which represents the real or imaginary relation:

$$\begin{aligned} \tilde{U}^{Re}_{[BC]} &= \tilde{U}^{Re}_{[AD]}cos(\frac{2\pi}{N}n) - \tilde{U}^{Im}_{[AD]}sin(\frac{2\pi}{N}n) \\ \tilde{U}^{Im}_{[BC]} &= \tilde{U}^{Re}_{[AD]}sin(\frac{2\pi}{N}n) + \tilde{U}^{Im}_{[AD]}cos(\frac{2\pi}{N}n) \end{aligned} \tag{48}$$

Eq. 48 can be represented by two identical meshes in Abaqus whose boundaries are coupled by the *MPC function in Abaqus. Similar to the derivation of Eq. 39, the transformation matrix Q can also be separated into real and imaginary parts based on Eq. 48.

$$\begin{bmatrix} U^{Re}_i \\ U^{Re}_{(CD)} \\ U^{Re}_{[AD]} \\ U^{Re}_{(AB)} \\ U^{Re}_{[BC]} \\ U^{Im}_i \\ U^{Im}_{(CD)} \\ U^{Im}_{[AD]} \\ U^{Im}_{(AB)} \\ U^{Im}_{[BC]} \end{bmatrix} = Q \begin{bmatrix} U^{Re}_i \\ U^{Re}_{(CD)} \\ U^{Re}_{[AD]} \\ U^{Re}_{(AB)} \\ U^{Im}_i \\ U^{Im}_{(CD)} \\ U^{Im}_{[AD]} \\ U^{Im}_{(AB)} \end{bmatrix} \tag{49}$$

where Q matrix is

$$\begin{bmatrix} \mathbf{I} & \mathbf{0} & \mathbf{0} & \mathbf{0} & \mathbf{0} & \mathbf{0} & \mathbf{0} & \mathbf{0} \\ \mathbf{0} & \mathbf{I} & \mathbf{0} & \mathbf{0} & \mathbf{0} & \mathbf{0} & \mathbf{0} & \mathbf{0} \\ \mathbf{0} & \mathbf{0} & \mathbf{I} & \mathbf{0} & \mathbf{0} & \mathbf{0} & \mathbf{0} & \mathbf{0} \\ \mathbf{0} & \mathbf{0} & \mathbf{0} & \mathbf{I} & \mathbf{0} & \mathbf{0} & \mathbf{0} & \mathbf{0} \\ \mathbf{0} & \mathbf{0} & [cos(\frac{2\pi}{N}n)] & \mathbf{0} & \mathbf{0} & -[sin(\frac{2\pi}{N}n)] & \mathbf{0} & \mathbf{0} \\ \mathbf{0} & \mathbf{0} & \mathbf{0} & \mathbf{0} & \mathbf{I} & \mathbf{0} & \mathbf{0} & \mathbf{0} \\ \mathbf{0} & \mathbf{0} & \mathbf{0} & \mathbf{0} & \mathbf{0} & \mathbf{I} & \mathbf{0} & \mathbf{0} \\ \mathbf{0} & \mathbf{0} & \mathbf{0} & \mathbf{0} & \mathbf{0} & \mathbf{0} & \mathbf{I} & \mathbf{0} \\ \mathbf{0} & \mathbf{0} & \mathbf{0} & \mathbf{0} & \mathbf{0} & \mathbf{0} & \mathbf{0} & \mathbf{I} \\ \mathbf{0} & \mathbf{0} & [sin(\frac{2\pi}{N}n)] & \mathbf{0} & \mathbf{0} & [cos(\frac{2\pi}{N}n)] & \mathbf{0} & \mathbf{0} \end{bmatrix} \tag{50}$$

The Bloch relations of forces are:

$$\begin{aligned} \tilde{F}^{Re}_{[BC]} &= -(\tilde{F}^{Re}_{[AD]} cos(\frac{2\pi}{N}n) - \tilde{F}^{Im}_{[AD]} sin(\frac{2\pi}{N}n)) \\ \tilde{F}^{Im}_{[BC]} &= -(\tilde{F}^{Re}_{[AD]} sin(\frac{2\pi}{N}n) + \tilde{F}^{Im}_{[AD]} cos(\frac{2\pi}{N}n)) \end{aligned} \tag{51}$$

We can also obtain the following relation by multiplying Eq. 47 by Q^T and using the above force Bloch relations and $F_i = 0$, $F_{(AB)} = 0$, and $F_{(CD)} = 0$:

$$Q^T \left(\begin{bmatrix} K & \mathbf{0} \\ \mathbf{0} & K \end{bmatrix} - \omega^2 \begin{bmatrix} M & \mathbf{0} \\ \mathbf{0} & M \end{bmatrix} \right) Q \begin{bmatrix} U^{Re}_i \\ U^{Re}_{(CD)} \\ U^{Re}_{[AD]} \\ U^{Re}_{(AB)} \\ U^{Im}_i \\ U^{Im}_{(CD)} \\ U^{Im}_{[AD]} \\ U^{Im}_{(AB)} \end{bmatrix} = Q^T \begin{bmatrix} 0 \\ 0 \\ F^{Re}_{[AD]} \\ 0 \\ F^{Re}_{[BC]} \\ 0 \\ 0 \\ F^{Im}_{AD} \\ 0 \\ F^{Im}_{[BC]} \end{bmatrix} = 0 \tag{52}$$

The calculation of ω^2 consists of two steps: a nonlinear static analysis (pre-buckling analysis) and a frequency analysis (eigenvalue analysis). In the static analysis the pre-buckling deformation of corrugated cylindrical shell has a periodicity of one unit cell, i.e. $\tilde{U}^{Re}_{[BC]} = \tilde{U}^{Re}_{[AD]}$ and $\tilde{U}^{Im}_{[BC]} = \tilde{U}^{Im}_{[AD]}$. Edge "AB" is fully clamped and the shell is compressed by applying a uniform axial end-shortening on edge "CD", i.e. $\tilde{U}^{Re}_{[AB]} = \tilde{U}^{Im}_{[AB]} = 0$ and $\tilde{U}^{Re}_{z,[CD]} = \tilde{U}^{Im}_{z,[CD]} = Uz$. Therefore, the load parameter λ in the previous discussion is $\lambda = |Uz|$.

In the frequency analysis the edge "AB" is fully clamped, i.e. $\tilde{U}^{Re}_{[AB]} = \tilde{U}^{Im}_{[AB]} = 0$. As discussed in the previous section, $\tilde{U}^{Re}_{[CD]}$ and $\tilde{U}^{Im}_{[CD]}$ are zero when $n > 0$ in order to satisfy the Bloch relation. For the case $n = 0$, the real and imaginary parts are not coupled and the only free degree of freedom of edge "CD" is the uniform translational displacement in the z (axial) direction.

B. Algorithm of Finding Critical Buckling Load

In principle, we need to run $\{N/2\} + 1$ simulations in order to find the lowest buckling load according to Eq. 42:

$$\lambda_{crit} = \min_{n=0,1,2,\ldots,\{N/2\}} (\lambda(n))$$

This process could be computationally expensive. We developed an algorithm to reduce the number of simulations required to find the lowest buckling load. Our algorithm consists of three major steps.

1. Step 1: Finding the Buckling Load for $n = 0$

Both the pre-buckling deformation and buckling modes for $n = 0$ have the periodicity of one unit cell, i.e. $\tilde{U}^{Re}_{[BC]} = \tilde{U}^{Re}_{[AD]}$ and $\tilde{U}^{Im}_{[BC]} = \tilde{U}^{Im}_{[AD]}$. The real and imaginary parts are not coupled in both static and frequency steps since the sine terms in Eq. 48 are zero. In the nonlinear static analysis, a corrugation of a shell is compressed by applying incremental uniform end-shortening until it reaches the bifurcation point B_0, as shown in the schematic Fig. 4. The increment containing the bifurcation point is further refined until the required accuracy is achieved. The detection of B_0 is based on the eigenvalues ω^2 obtained from the frequency analysis. Four possible situations could happen.

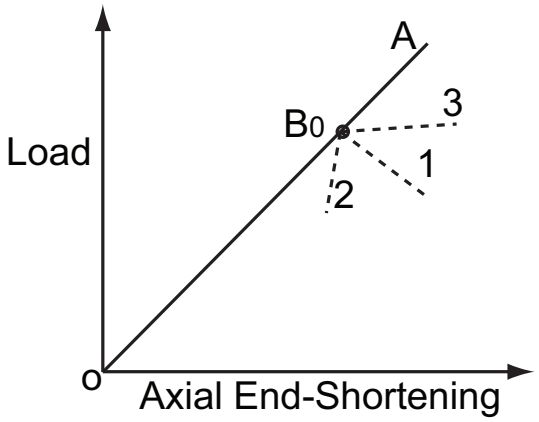

Figure 4: Schematic of possible post-buckling branches. B_0 is the bifurcation point corresponding the branch of $n = 0$.

Even though nonlinear analysis is used for the static step, it is still possible that the shell stays on the primary branch $B_0 - A$ when the load exceeds the bifurcation point. The shell is in an unstable state as it has passed the bifurcation points. The shell is not stable either if it is on the bifurcated branch $B_0 - 1$. Therefore, the eigenvalues ω^2 obtained for the points on branches $B_0 - A$ and $B_0 - 1$ are negative. B_0 can be accurately found by checking the change of signs of the eigenvalues during the loading.

The branch $B_0 - 2$ is also unstable. The shell is subject to displacement controlled loading ($\lambda = |Uz|$) in the static step and the applied compressive end-shortening incrementally increases. Hence, the shell can never reach the branch $B_0 - 2$. The increments of the nonlinear static analysis are set to automatically decrease in order to find the equilibrium state. Therefore, the shell can reach a very close vicinity of B_0. The last point on the primary branch is used as the bifurcation point.

B_0 is relatively difficult to find for the case of stable post-buckling branch $B_0 - 3$ because its eigenvalues are still positive and B_0 cannot be found by checking the change of signs of eigenvalues. The eigenvalue decreases dramatically when the load is close to the bifurcation point and it increases from zero when the load exceeds B_0 and goes onto branch $B_0 - 3$. In addition, the slope of the load-displacement curve is different for the primary and secondary branches. These two signatures are used to determine if the shell is in the stable post-buckling state. Since all eigenvalues except that of the bifurcation point are all positive on $O - B_0 - 3$, we use the point with largest slope change, i.e. largest curvature, on the load-displacement curve as the bifurcation point, instead of finding the point with zero eigenvalue which is operationally very difficult for this case.

2. Step 2: Sorting other n's According to Eigenvalues

We can use the location of B_0 obtained in step 1 to filter and sort the other n's for further simulations. Fig. 5 is a schematic for this process. If the load of B_0 is larger than the buckling load of a certain branch, e.g. n_1, n_2, and n_k in Fig. 5, the eigenvalues corresponding to the coupled boundaries of Eqs. 48 for these n's are guaranteed to be negative. If the eigenvalues are positive, then the load of B_0 is smaller than the buckling load of these branch, e.g. n_j in Fig. 5, and no further calculations are need since we are only interested in the lowest buckling load. The critical buckling mode is among the n's with negative eigenvalues and they are sorted increasingly according to their eigenvalues. The n with lowest eigenvalue is more likely to be

the critical one. It should be noted that this is not a rigorous assumption; however, it can provide useful information in order to find the critical n as fast as possible.

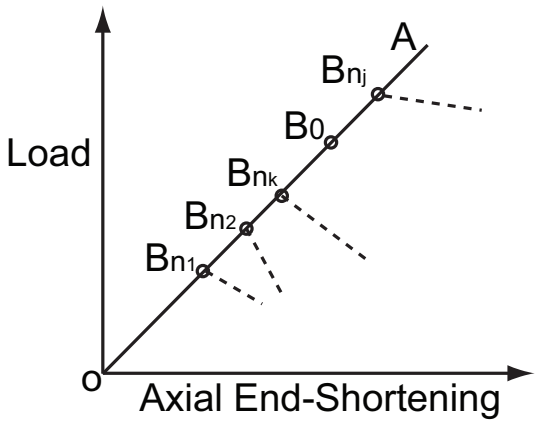

Figure 5: Schematic of the bifurcation points on the primary branch. B_{n_k} is the bifurcation point when $n = n_k$.

3. Step 3: Finding the Critical Buckling Load

As discussed in step 2, the sign of eigenvalues is always negative if the load has passed the bifurcation point B_{n1}. Hence, change of signs of eigenvalues can be used to detect B_{n1}. The increment containing B_{n1} is iteratively refined until it reaches the required accuracy. We then check the eigenvalues of $n_2, n_3, ..., n_k$ on the load of B_{n1} and sort them according to their eigenvalues (step 2). If there exist other n's with negative eigenvalues, the one with lowest eigenvalue is then analyzed to find its buckling load (step 3). Steps 2 and 3 are repeated until the critical load λ_{cirt} corresponding to the critical branch n_{crit} is found. The eigenvalue of λ_{cirt} is zero for n_{crit} and positive for all other n's. The buckling modes of the whole structure are then obtained through Eq. 23.

This algorithm can avoid unnecessary simulations as much as possible so as to reduce the computational time. The frequency analyses are independent with each other. Therefore, they can be carried out in a parallel way. The parallel computation of frequency analyses can further reduce the computational time.

V. Validation

We applied our modified Bloch wave method in the buckling analyses of corrugated cylindrical shells in order to validate the method. Both linear and nonlinear analyses of detailed full finite element models are also carried out, and their results and computational time are compared to the modified Bloch wave method.

A. Corrugated Composite Cylindrical Shells

The corrugations are sinusoidal and the cross-sections were obtained by superposing a sinusoidal wave on a reference circle:

$$r(\phi) = R + \Delta r \sin(N\phi), \tag{53}$$

where N is the total number of corrugations and Δr their amplitude. In this paper, the number of corrugations N is chosen as $N = 12, 13, 16, 17, 19, 22, 23, 34, 25, 26, 29, 30, 31, 32, 37, 40$

The shells were chosen to have a square aspect ratio. The dimensions presented in Table 1 were chosen.

A symmetric six-ply laminate, $[+60°, -60°, 0°]_s$ was adopted, and 0° direction is shell axial direction. It consisted of 30 μm thick unidirectional laminae of T800 carbon fibers and ThinPreg 120EPHTg-402 epoxy, provided by the North Thin Ply Technology company, with a fiber volume fraction of approximately 50%. The following lamina properties were measured: $E_1 = 127.9$ GPa, $E_2 = 6.49$ GPa, $G_{12} = 7.62$ GPa, and $\nu_{12} = 0.354$, where E_1 is the modulus along the fiber direction. The ABD matrix of the laminate was calculated from these properties, using classical lamination theory:

Table 1: Dimensions of wavy shell designs

Thickness, t	180 μm
Radius, R	35 mm
Length L	70 mm
Maximum deviation from circle, Δr	1.5 mm

$$ABD = \begin{pmatrix} 9.919 \times 10^6 & 2.670 \times 10^6 & 0 & 0 & 0 & 0 \\ 2.670 \times 10^6 & 9.919 \times 10^6 & 0 & 0 & 0 & 0 \\ 0 & 0 & 3.625 \times 10^6 & 0 & 0 & 0 \\ 0 & 0 & 0 & 0.0108 & 0.0099 & 0.0034 \\ 0 & 0 & 0 & 0.0099 & 0.0373 & 0.0081 \\ 0 & 0 & 0 & 0.0034 & 0.0081 & 0.0125 \end{pmatrix} \tag{54}$$

where the units of the A and D matrices are N/m and Nm, respectively.

B. Results and Comparison

Around 1,500 S4 fully integrated shell elements were used for a corrugation in the Bloch wave method. Both linear and nonlinear analyses of detailed full finite element models were carried out. The full finite element models have the same element size as the models in the Bloch wave method. All simulations were run on a Xeon X5680 server with 12 CPUs on a single motherboard.

The linear eigenvalue analysis *Buckle function of Abaqus was used for linear buckling analysis. Abaqus offers the Lanczos and the subspace iteration eigenvalue extraction methods. It was found that the Lanczos method was much slower than the subspace method and it failed to solve the eigenvalue problem for the shells with more than 23 corrugations. Therefore, the subspace method was used for the linear buckling analysis. As discussed in the previous sections, there are two coincided buckling modes for the cases $n > 0$. It was found that the subspace method could provide an inaccurate second buckling mode and load if the number of extracted eigenvalues is too small. Therefore, we extracted the first 10 eigenmodes although we are only interested in the first two buckling modes. We found that this setup was able to provide accurate second buckling modes.

The nonlinear analyses of full detailed finite element models consisted of two steps, similar to the Bloch wave method, that are a nonlinear static analysis and a frequency analysis. The shells were first compressed by applying a uniform end-shortening at one end, and then a frequency step was carried out to find the eigenvalue ω^2 corresponding to this stress state. The critical buckling load was found when the eigenvalue ω^2 decreased to zero. The frequency analyses are independent with each other so they were performed in a parallel way.

The critical axial end-shortening obtained from the Bloch wave method, nonlinear and linear full finite element analyses are plotted in Fig. 6. The buckling loads are plotted in Fig. 7. In the linear analysis the end-shortening is extracted as the eigenvalue. Therefore, the critical loads were not obtained for linear analysis. The results obtained from the Bloch wave method and the linear full finite element analyses are compared to the ones obtained from the nonlinear full finite element analyses. Figs. 6 and 7 show that all buckling loads and critical end-shortening are very close. It is found that their differences are less than 0.5%.

The buckling modes obtained from the Bloch wave method, linear and nonlinear full model analysis for $N = 13, 31, 40$ are plotted in Figs. 8, 9 and 10. The buckling is local for $N <= 30$ and global for $N >= 31$. These figures show that the Bloch wave method can capture both local and global buckling and the buckling modes match the results obtained from the nonlinear full model analyses. Although the linear full model analysis can provide accurate buckling loads, it cannot obtain correct buckling modes for some cases, as seen in Fig. 9 (c).

The computational time for these three methods is plotted in Fig. 11. It can be seen that the computational time of the nonlinear analysis increased linearly with respect to the number of corrugations. For

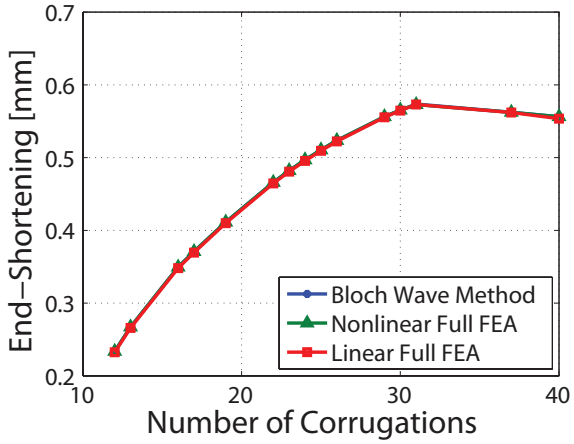

Figure 6: Critical end-shortening obtained from the Bloch wave method, nonlinear and linear full finite element analyses.

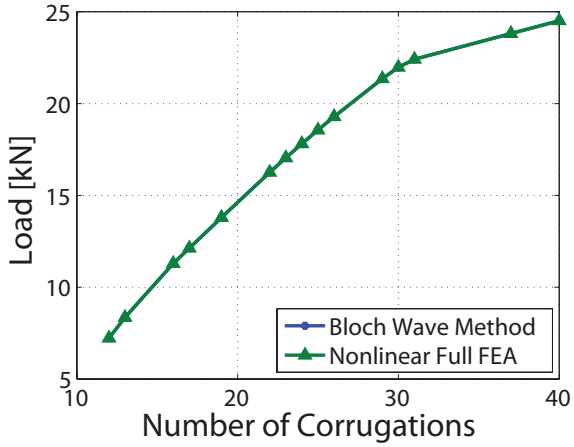

Figure 7: Critical buckling loads obtained from the Bloch wave method, nonlinear and linear full finite element analyses.

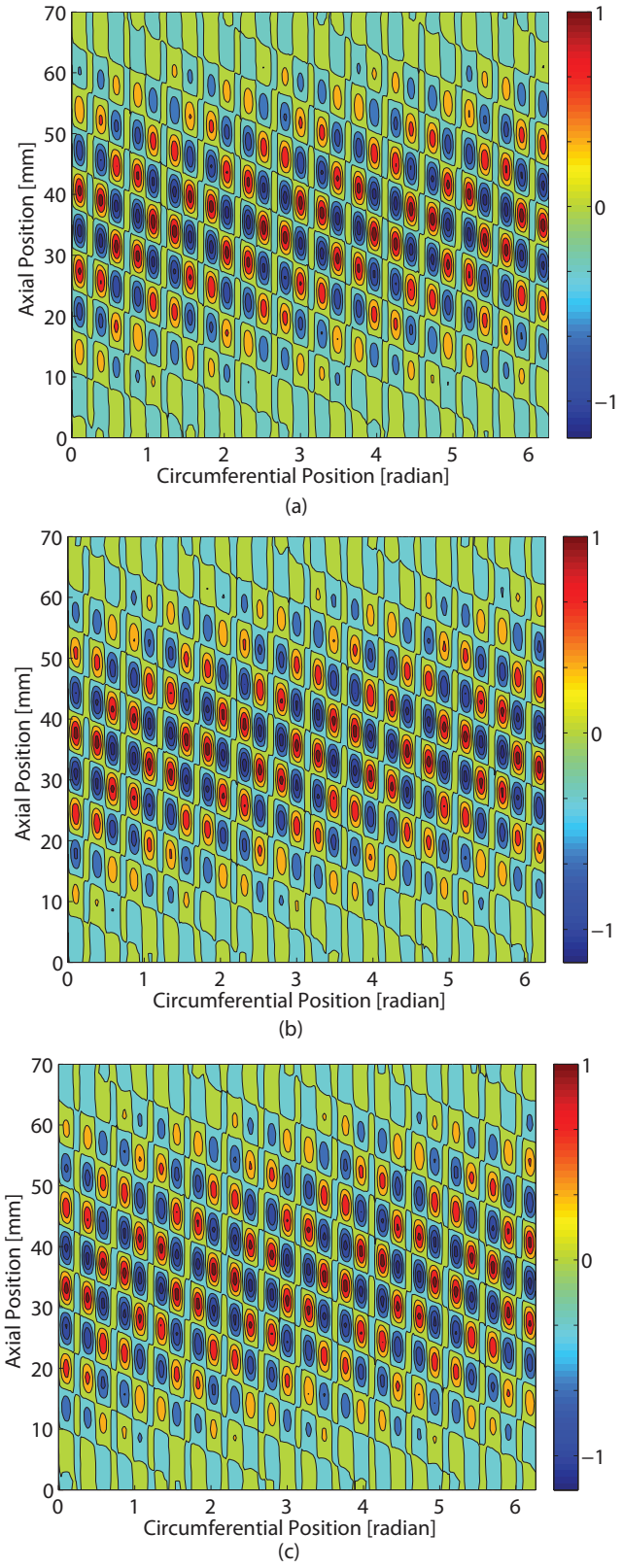

Figure 8: Buckling modes of the shell with $N = 13$ corrugations obtained from (a) Bloch wave method, (b) nonlinear full finite element model, and (c) linear full finite element model.

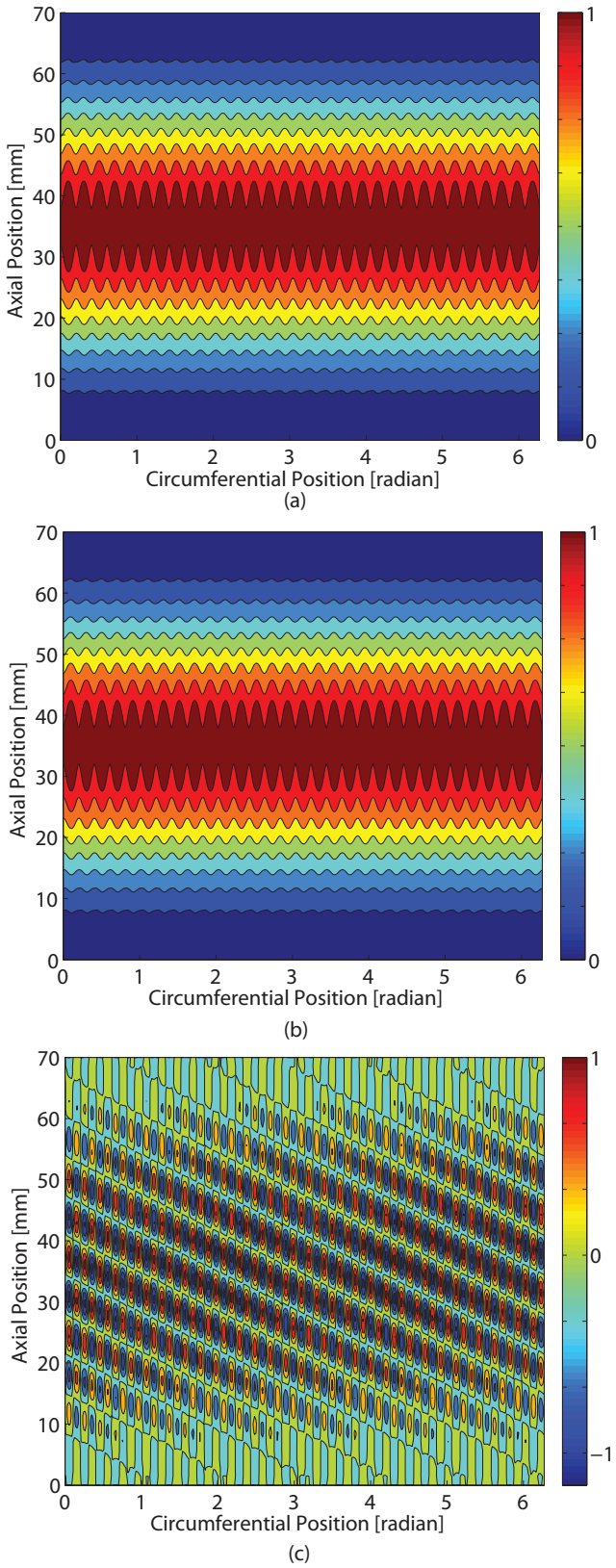

Figure 9: Buckling modes of the shell with $N = 31$ corrugations obtained from (a) Bloch wave method, (b) nonlinear full finite element model, and (c) linear full finite element model.

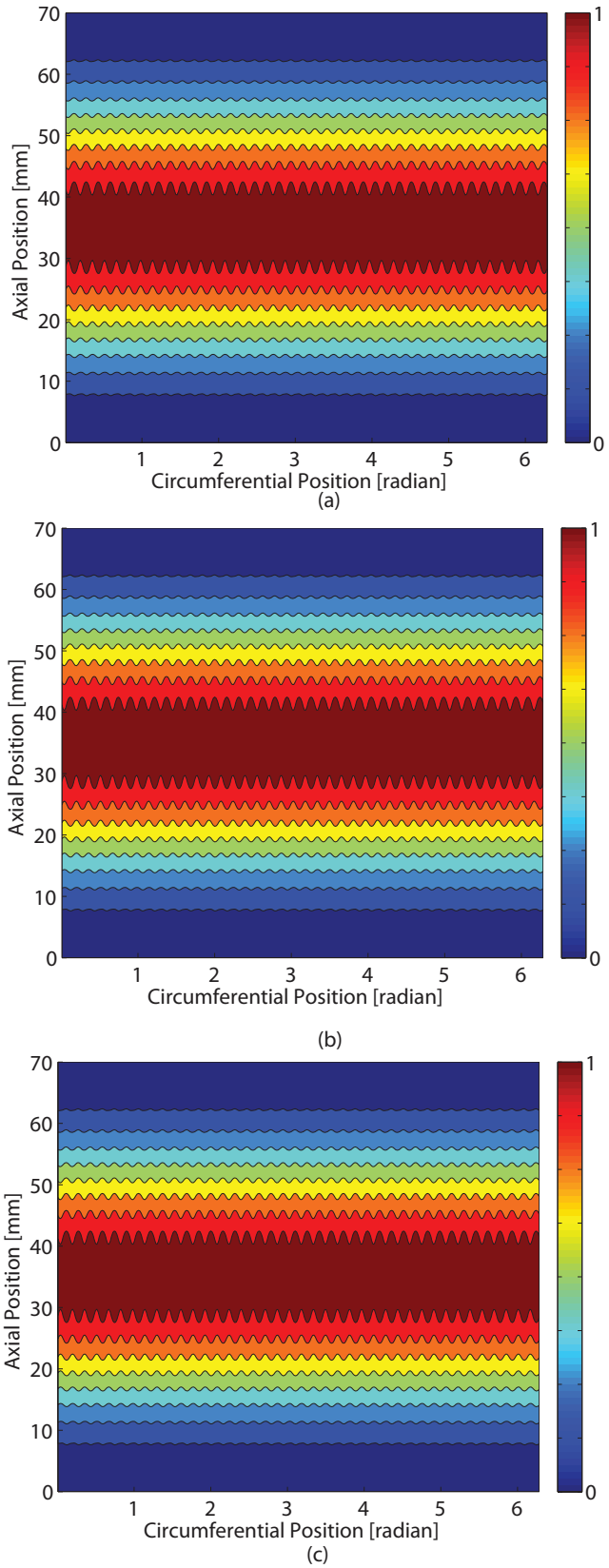

Figure 10: Buckling modes of the shell with $N = 40$ corrugations obtained from (a) Bloch wave method, (b) nonlinear full finite element model, and (c) linear full finite element model.

linear analysis, the computational time increased faster for larger number of corrugations and it was just slightly smaller than the nonlinear analysis for $N = 40$. However, the computational time of the Bloch wave method did not scale up as the number of corrugations increased.

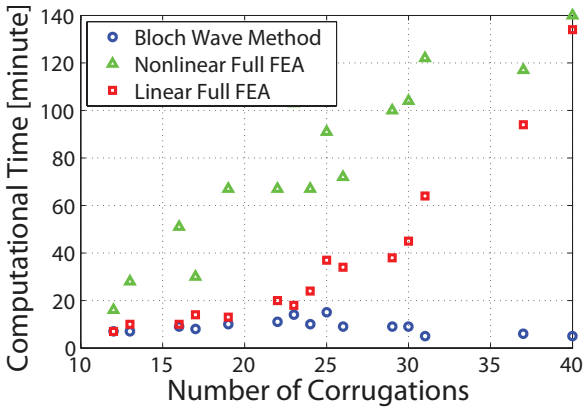

Figure 11: Computation time for the Bloch wave method, linear and nonlinear full finite element analyses.

VI. Conclusion

We have developed an efficient computational method for the buckling analysis of corrugated cylindrical shells which builds on the Bloch wave method and the stiffness matrix method of rotationally periodic structures. The traditional Bloch wave method is applicable for the buckling analysis of infinitely 2- or 3-dimensional periodic structures. We modified the Bloch wave method in order to analyze the buckling behavior of rotationally periodic shell structures such as corrugated cylindrical shells. The Bloch wave method involves the computation of complex-valued displacement fields. Following the work by Aberg and Gudmundson [28] and Bertoldi et. al. [25,29], we set up two identical meshes in Abaqus to represent the real and complex fields and their boundaries were coupled according to the Bloch relations. We also developed an algorithm to efficiently perform the Bloch wave method for corrugated cylindrical shells.

We used our modified Bloch wave method to analyze the onset of buckling for a range of composite corrugated cylindrical shells. Linear and nonlinear analyses based on detailed full finite element models were also performed in order to validate our method. It was shown that our modified Bloch wave method can achieve highly accurate results. Compared to the nonlinear full finite element analyses, the errors of the buckling loads obtained by our method are smaller than 0.5% for all analyzed corrugated shells. In addition, our method was able to accurately capture both global and local buckling modes.

The computational time required by our modified Bloch wave method did not scale up as the number of corrugations increased. However, both linear and nonlinear full finite element analyses required much higher computational time for heavily corrugated shells than lightly corrugated ones. The reduction of computation time of our method is due to three reasons. First, the Bloch wave method was performed on a single corrugation rather than on the whole corrugated shell, reducing the size of finite element model. Second, the prediction of the critical buckling loads and modes was separated into a series of small eigenvalue problems which were carried out in a parallel way. Third, the algorithm we developed to perform our modified Bloch wave method was able to avoid unnecessary simulations.

It should be noted that the Bloch wave method is applicable to the prediction of onset of buckling and it cannot be used to find the post-buckling behavior. The Bloch wave analysis is performed on a unit repetitive portion of a periodic structure. Therefore, predicting the onset of buckling for imperfect structures using the Bloch wave method is also a challenge due to the random nature of imperfections. It is common to use a buckling mode as the shape of imperfection. It is possible to use the Bloch wave method to study the imperfection-sensitivity of structures if the assumed shape of imperfection is periodic. Otherwise detailed full finite element models are necessary for analyzing the imperfection-sensitivity.

Acknowledgments

We thank Dr. Katia Bertoldi for providing her presentations in the 2014 CISM short courses. We also thank Drs. Francisco López Jiménez and Ryan Elliott for helpful discussions on the Bloch wave method.

References

[1]Johnson Jr, R., "Design and Fabrication of a Ring-Stiffened Graphite-Epoxy Corrugated Cylindrical Shell", NASA CR-3026, 1978.

[2]Yokozeki, T., Takeda, S., Ogasawara, T., Ishikawa, T., "Mechanical Properties of Corrugated Composites for Candidate Materials of Flexible Wing Structures", Composites Part A: Applied Science and Manufacturing, Vol. 37, Issue 10, pp. 1578-1586, 2006.

[3]Thill, C., Etches, J. A., Bond, I. P., Potter, K. D., Weaver, P. M., and Wisnom, M. R., "Investigation of Trapezoidal Corrugated Aramid/Epoxy Laminates under Large Tensile Displacements Transverse to the Corrugation Direction", Composites Part A: Applied Science and Manufacturing, Vol. 41, Issue 1, pp. 168-176, 2010.

[4]Bisagni, C., and Vescovini, R. "Fast Tool for Buckling Analysis and Optimization of Stiffened Panels", Journal of Aircraft, Vol. 46, No. 6, 2041-2053, 2009.

[5]Block, D. L., Card, M. F., and Mikulas Jr, M. M. "Buckling of Eccentrically Stiffened Orthotropic Cylinders", NASA-TN-D-2960, 1965.

[6]Amazigo, J. C., and J. W. Hutchinson. "Imperfection-Sensitivity of Eccentrically Stiffened Cylindrical Shells", AIAA Journal Vol. 5, No.3, pp. 392-401, 1967.

[7]Simitses, G. J., "General Instability of Eccentrically Stiffened Cylindrical Panels, Journal of Aircraft, Vol. 8, No. 7, pp. 569575, 1971.

[8]Calladine, C. R. "Theory of Shell Structures", Cambridge University Press. 1989.

[9]Briassoulis, D. "Equivalent Orthotropic Properties of Corrugated Sheets", Computers and Structures, Vol. 23, No. 2, pp. 129-138, 1986.

[10]Liew, K. M., Peng, L. X., and Kitipornchai, S. "Nonlinear Analysis of Corrugated Plates using a FSDT and a Meshfree Method", Computer Methods in Applied Mechanics and Engineering, Vol. 196, No. 21, pp. 2358-2376, 2007.

[11]Xia, Y., Friswell, M. I., and Flores, E. I. "Equivalent Models of Corrugated Panels", International Journal of Solids and Structures, Vol. 49, No. 13, pp. 1453-1462, 2012.

[12]Ye, Z., Berdichevsky, V. L., and Yu, W., "An equivalent classical plate model of corrugated structures", International Journal of Solids and Structures, Vol. 51, Issue 11, pp. 2073-2083, 2014.

[13]Lamberti, L., Venkataraman, S., Haftka, R. T., and Johnson, T. F. "Preliminary Design Optimization of Stiffened Panels using Approximate Analysis Models", International Journal for Numerical Methods in Engineering, Vol. 57, No. 10, pp. 1351-1380, 2003.

[14]Wittrick, W. H., and Williams, F. W. (1974). Buckling and vibration of anisotropic or isotropic plate assemblies under combined loadings. International Journal of Mechanical Sciences, 16(4), 209-239.

[15]Anderson, M. S., Williams, F. W., and Wright, C. J. (1983). Buckling and vibration of any prismatic assembly of shear and compression loaded anisotropic plates with an arbitrary supporting structure. International Journal of Mechanical Sciences, 25(8), 585-596.

[16]Williams, F. W., and Anderson, M. S. (1983). Incorporation of Lagrangian multipliers into an algorithm for finding exact natural frequencies or critical buckling loads. International journal of mechanical sciences, 25(8), 579-584.

[17]Williams, F. W., Anderson, M. S., Kennedy, D., Butler, R., and Aston, G.. (1990). VICONOPT-Program for exact vibration and buckling analysis or design of prismatic plate assemblies. NASA CR-181966.

[18]J. Singer, J. Arbocz, and T. Weller. Buckling Experiments: Experimental Methods in Buckling of Thin-Walled Structures: Vol. 2. New York: Wiley, 2002.

[19]Williams, F. W. (1986). An algorithm for exact eigenvalue calculations for rotationally periodic structures. International journal for numerical methods in engineering, 23(4), 609-622.

[20]Williams, F. W. (1986). Exact eigenvalue calculations for structures with rotationally periodic substructures. International journal for numerical methods in engineering, 23(4), 695-706.

[21]Geymonat, G., Mller, S., and Triantafyllidis, N. (1993). Homogenization of nonlinearly elastic materials, microscopic bifurcation and macroscopic loss of rank-one convexity. Archive for rational mechanics and analysis, 122(3), 231-290.

[22]Triantafyllidis, N., and Schnaidt, W. C. (1993). Comparison of microscopic and macroscopic instabilities in a class of two-dimensional periodic composites. Journal of the Mechanics and Physics of Solids, 41(9), 1533-1565.

[23]Triantafyllidis, N., and Schraad, M. W. (1998). Onset of failure in aluminum honeycombs under general in-plane loading. Journal of the Mechanics and Physics of Solids, 46(6), 1089-1124.

[24]Lpez Jimnez, F., and Triantafyllidis, N. (2013). Buckling of rectangular and hexagonal honeycomb under combined axial compression and transverse shear. International Journal of Solids and Structures, 50(24), 3934-3946.

[25]Bertoldi, K., Boyce, M. C., Deschanel, S., Prange, S. M., and Mullin, T. (2008). Mechanics of deformation-triggered pattern transformations and superelastic behavior in periodic elastomeric structures. Journal of the Mechanics and Physics of Solids, 56(8), 2642-2668.

[26]Gong, L., Kyriakides, S., and Triantafyllidis, N. (2005). On the stability of Kelvin cell foams under compressive loads. Journal of the Mechanics and Physics of Solids, 53(4), 771-794.

[27]Kittel, C. and McEuen, P. (1976). Introduction to solid state physics (Vol. 8). New York: Wiley.

[28]Aberg, M. and Gudmundson, P. (1997). The usage of standard finite element codes for computation of dispersion relations in materials with periodic microstructure. The Journal of the Acoustical Society of America, 102(4), 2007-2013.

[29]Shim, J., Shan, S., Komrlj, A., Kang, S. H., Chen, E. R., Weaver, J. C., and Bertoldi, K. (2013). Harnessing instabilities for design of soft reconfigurable auxetic/chiral materials. Soft Matter, 9(34), 8198-8202.

[30]Wang, D., and Abdalla, M. (2014). Global and local buckling analysis of grid-stiffened composite panels. Composite Structures. In press.

[31]Virgin, L. N. (2007). Vibration of axially loaded structures (Vol. 393). New York: Cambridge University Press.